Circuit Loading in Radio-Frequency Current Measurements: The Insertion Impedance of the Transformer Probes.

Article · January 2010

Source: DBLP

CITATIONS
6

READS
529

2 authors, including:

Carlo F. M. Carobbi
University of Florence
83 PUBLICATIONS **346** CITATIONS

SEE PROFILE

Circuit Loading in Radio-Frequency Current Measurements: The Insertion Impedance of the Transformer Probes

Carlo F. M. Carobbi, *Member, IEEE*, and Luigi M. Millanta

***Abstract*—Considerable inaccuracy can be introduced in RF current measurements through loading effects from the transformer-type RF current probes. A physical model, which consists of a lumped impedance in series with the flow of the current under measurement, is obtained. The correlation between the loading (insertion) impedance and the geometrical and physical characteristics of the probe is clearly described through formulas that are useful for design purposes. The model is compared with those existing in the technical literature, and the main differences are highlighted and discussed. The theoretical predictions are experimentally confirmed. A direct application of the concepts discussed here to the improvement of the accuracy of the V/I-type vector impedance measurements is also shown. This paper is an extended version of the work by Carobbi and Millanta, including a more detailed description of mathematical derivations and experimental results and an updated list of references.**

***Index Terms*—Bulk-current injection (BCI) probe, current probe, electromagnetic compatibility (EMC), insertion impedance, loading effect, RF.**

I. Introduction

THIS paper analyzes the perturbation produced by the transformer current probes in terms of an equivalent impedance appearing in series with the circuit being probed. We will refer to this equivalent series impedance as the "insertion impedance." Although this parameter is of dominant importance (second only to the probe transfer impedance), it has not received proportionally adequate attention in the literature. Two different circuit models of the insertion impedance exist for the current and the bulk-current injection (BCI) probes: one is presented in [2], and the other is described in the operating manuals of various probes (see, for example, [3]). The behavior of the absolute value is exactly equivalent between the two; however, the predicted insertion impedances differ at high frequencies *being their phases opposite*. Various manufacturers simply offer graphs that describe the typical magnitude versus frequency, and agreement with the results from the two models is observed. The scope of this paper is to gain insight into the physical properties and to show how, in a specific application, the frequency behavior of the series parasitic impedance of a typical vector impedance meter (VIM) can accurately be described in terms of the insertion impedance of its current-sensing circuit. Equations describing the frequency dependence of the parasitic resistance and inductance of the meter are here derived, thus permitting to automatically correct for the corresponding systematic errors through computation. This detailed predictive capability can be deemed to increase confidence in the operation of the instrument.

Manuscript received May 13, 2008; revised January 13, 2009. First published August 18, 2009; current version published December 9, 2009. The Associate Editor coordinating the review process for this paper was Dr. Gerd Vandersteen.

The authors are with the Department of Electronics and Telecommunications, University of Florence, 50139 Florence, Italy (e-mail: carlo.carobbi@unifi.it).

Digital Object Identifier 10.1109/TIM.2009.2022450

II. Previous Results

RF current probes and BCI probes have assumed a large importance mainly because of their widespread use in electromagnetic compatibility (EMC) emission and susceptibility testing (see [4]). In a larger sense, the importance of current measurements is obvious in all the branches of electrical applications. In spite of this, little space is devoted in textbooks and technical notes to these devices, particularly in relation to any effort for an in-depth analysis of the physical aspects. Some fundamental properties are derived and experimentally demonstrated in the tutorial papers [2], [5]. Almost all the literature, both technical and scientific, is concerned with the derivation of the calibration parameter of the probe, i.e., the transfer impedance (current probe) and the insertion loss (BCI probe). In particular, recent publications (see [6] and [7]) describe and analyze the problems arising from the calibration of the probe at very high frequencies (up to 1 GHz).

Little material exists describing the loading effect. The basic EMC standard CISPR 16-1 [8] specifies the essential electrical characteristics of EMC current probes and describes in some detail a possible realization scheme. A maximum allowable insertion impedance of 1 Ω (absolute) is specified, but the needed design criteria to comply with this specification are not elucidated.

A. Basic Theory

The loading effect is analyzed in [2], where the (magnetic) loading effects giving rise to insertion impedance and the (electric) capacitive loading are separately discussed. The insertion impedance Z_{ins} is the impedance appearing in series with the conductor under test (the primary) when the probe and its load are in place. The insertion impedance comes from the sum of two contributions: 1) the secondary impedance reflected into the primary by transformer action Z_{refl} and 2) the intrusion impedance originating from the introduction of an extraneous material (mainly the core magnetic material) inside the primary circuit Z_{intr}.

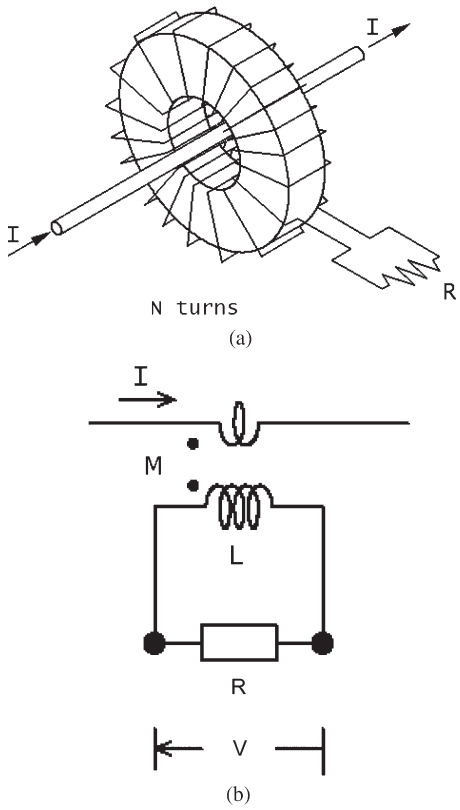

Fig. 1. (a) Schematic representation of an RF current probe. (b) Equivalent circuit model.

The probe [see Fig. 1(a)], which is an N-turns coil, embraces the conductor (CUT) carrying the current under measurement I and is closed on the resistive load R (often the 50 Ω input resistance of the measuring receiver). The circuit model is shown in Fig. 1(b), where M represents the mutual coupling between the probe and the CUT, and L is the self-inductance of the probe winding. The reflected impedance is given by [9, eq. 3–20].

$$Z_{\text{refl}} = \frac{(\omega M)^2}{R + j\omega L} \tag{1}$$

whereas the intrusion impedance is [2]

$$Z_{\text{intr}} = j\omega \frac{L}{N^2} - j\omega \frac{L_0}{N^2} \tag{2}$$

where L_0 is the inductance the winding would have in a vacuum, i.e., $L_0 = L/\mu_r$, and μ_r is the relative permeability of the core magnetic material ($\mu_r \gg 1$). Observe the second right term in (2). It can be seen to represent the amount of flux removed from the primary circuit in the volume occupied by the probe (experimentally verified, not reported here). When the probe winding geometry is close to the axial symmetry, it is seen that $L = NM$ [2]. The inductance of the winding is $L = N^2\mu_0\mu_r\Sigma/(2\pi\hat{R})$, where Σ is the toroid cross section, and $\hat{R}$ is the radius corresponding to the average flux density in the cross section. In the current technical applications, the toroid cross section is rectangular with axial length P, internal radius R_i, and external radius R_e, and the formula becomes

$$L = N^2 \frac{\mu_0\mu_r}{2\pi} P \ln(R_e/R_i). \tag{3}$$

Then, the insertion impedance is given by

$$\begin{aligned} Z_{\text{ins}} &= Z_{\text{refl}} + Z_{\text{intr}} \\ &= \frac{1}{N^2} \frac{R \cdot j\omega L}{R + j\omega L} - \frac{j\omega L_0}{N^2}. \end{aligned} \tag{4}$$

The resistive losses in the probe are neglected. The reasons for neglecting the nonideal effects connected with the possible losses of various origin are essentially the same as those commonly adopted when treating the basic operation of the probe, and we are here treating a second-order behavior effect of that probe. Basically, however, the acceptability of the lossless assumption is based on the fact that in practical operation, the device is essentially short circuited ($R \ll \omega L$), so the flux density inside the core is negligible (negligible core losses), and the conductor losses are negligible compared with the load resistance R (typically $R = 50\ \Omega$). On the other hand, in the low-frequency range ($R \gg \omega L$), the core losses are negligible, and conductor losses are even more negligible than in the high-frequency range.

Two characteristic frequencies are seen in equation (4), i.e.,

$$f_{c1} = \frac{1}{2\pi} \frac{R}{L} \tag{5}$$

$$f_{c2} = \frac{1}{2\pi} \frac{R(1 - L_0/L)}{L_0}. \tag{6}$$

The term corresponding to a negative inductance in (4) dominates above f_{c2} and gives rise to the characteristic high-frequency behavior, which proportionally increases to f. In the range above f_{c2}, the inductance of the circuit under test is effectively reduced by L_0. It is immediately seen that above f_{c2}, the value of $|Z_{\text{ins}}|$ can far exceed the usually expected value R/N^2.

B. Experimental Confirmation and Discussion

The overall behavior is better explained with reference to an actual experiment (see Fig. 2). Magnitude and phase are plotted as derived from (4) (continuous line), assuming measured or computed values of the parameters (no fitting). The corresponding measured values at 22 spot frequencies are shown as dotted circles. A toroidal ferrite core is adopted with the following nominal data: inner radius $R_i = 11.4$ mm, outer radius $R_e = 17.8$ mm, axial length $P = 12.7$ mm, and relative permeability $\mu_r = 127$ (nominal). In addition, we had $N = 10$, with measured inductance $L = 11.1$ μH, $L_0/N^2 = 1.1$ nH [as computed from core dimensions, equation (3)], and load resistance 47 Ω (nominal). Hence, from (5) and (6), we have $f_{c1} = 674$ kHz and $f_{c2} = 67.3$ MHz, and $R/N^2 = 0.47\ \Omega$.

The measurements on a primary circuit were performed with a VIM (400 kHz–100 MHz, injected current 100 μA) before and after the insertion of the probe. The primary circuit used in the experiments was mechanically and electrically quite similar to the commercially available current or BCI probe calibration fixtures. An example of the test jig is shown in Fig. 3. The agreement with the frequency behavior predicted by (4) is well within the experimental uncertainties. The root-mean-square (RMS) deviation between measurements and predictions is 81 mΩ (amplitude) and 5.3° (phase).

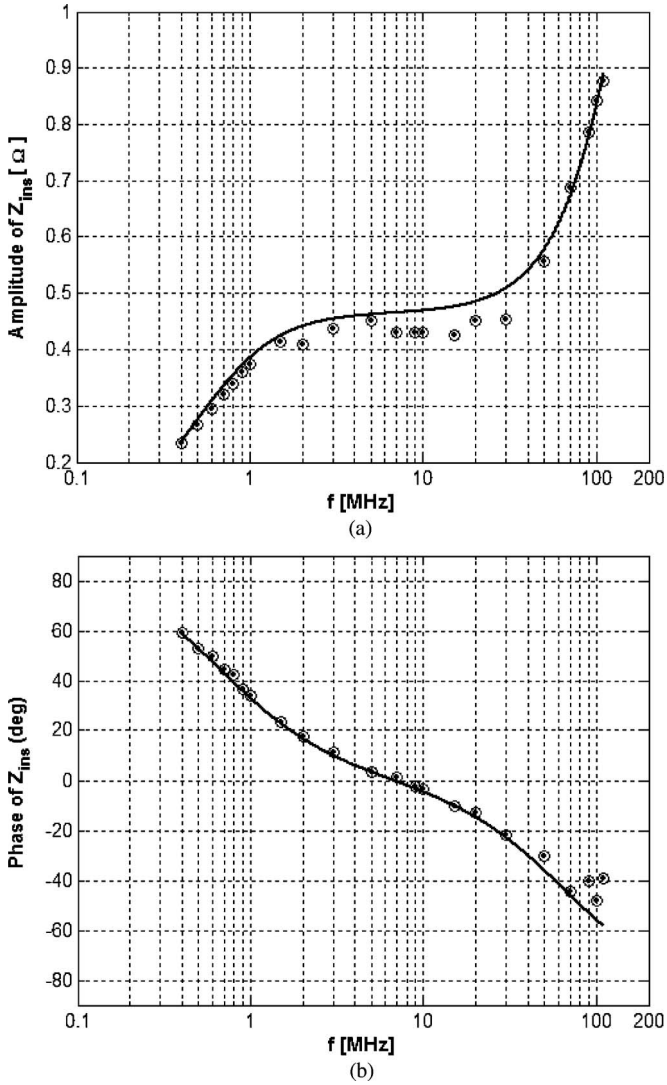

Fig. 2. (a) Magnitude and (b) phase of the insertion impedance of a current probe. Comparison between measurements (dotted circles) and theory (from (4), solid line). Probe data in the text.

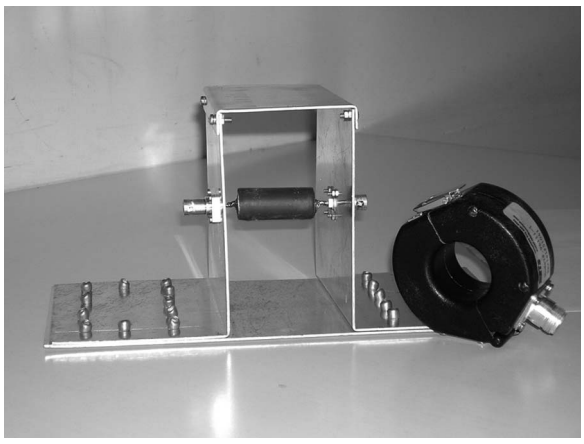

Fig. 3. Empty insertion: loss test jig. A current probe is shown on a side for visual comparison.

The magnitude of the insertion impedance does not depend on the sign of the $j\omega L_0/N^2$ term in (4). This term, however, dominates the insertion impedance at high frequencies, and in particular, the phase becomes negative. Often, the loading effect is simply given as a band-center impedance value, i.e., the resistance coupled into the primary R/N^2. In [3] and [10], a more detailed equivalent circuit of the insertion impedance is provided as the parallel of a resistance and an inductance, with an inductance of lesser value placed in series to the parallel.

With the numerical values offered, the result of the prediction of the model proposed in [3] and [10] is qualitatively and quantitatively consistent with (4) with one exception, that is, the reversal in the sign of the small series inductance. Thus, if we plot the magnitude of the insertion impedance as predicted in [10], we exactly obtain the same shape (same zero-pole zero sequence) as that predicted by (4). The phase in the high-frequency range (above f_{c2}) is, however, inverted. It is to be remarked that in cases where reactance terms comparable in magnitude with the negative term in (4) are present, the sign will be important, e.g., when influencing the possible resonance phenomena.

It can be observed in Fig. 2(b) that the agreement between predicted and measured phase tends to be less satisfactory, approaching the high-frequency limit. This can be attributed to the onset of additional loss phenomena not included in the model (hysteresis, eddy currents in the core material). It is also to be noted that the model appropriately works only if the relaxation frequency of the magnetic material is higher than f_{c2}.

III. Insertion Impedance in RF Impedance Measurements

Probe loading can determine to a significant extent the parasitic impedance terms introduced when measuring high-frequency impedances. In at least one important case, a current probe is incorporated in the architecture of a V/I-type high-quality VIM. For clarity, we will denote the complete probe head of the instrument as the "head," whereas the term "probe" will be reserved for the current-measuring transformer.

Interesting properties are derived from the treatment in this section and are described in Fig. 4, where the frequency behavior of the parasitic series resistance R_S and inductance L_S of a popular VIM[1] is plotted. The theoretical derivation is as follows: The properties of the measured series parasitic impedance can be interpreted by considering that the VIM senses the current flowing into the impedance under measurement by means of an RF current probe mounted inside the head body. The impedance Z_S measured by the VIM when short circuited at its head terminals is the sum of the impedance Z_P of the primary loop (i.e., the loop existing inside the head body plus some inductance contribution from the short-circuiting connection across the terminals) plus $Z_{\rm ins}$. We, therefore, have

$$Z_S = R_S + j\omega L_S = Z_P + Z_{\rm ins}. \tag{7}$$

We assume an essentially inductive primary impedance, that is,

$$Z_P = j\omega L_P. \tag{8}$$

[1]Hewlett and Packard model 4193A, 400 kHz to 110 MHz.

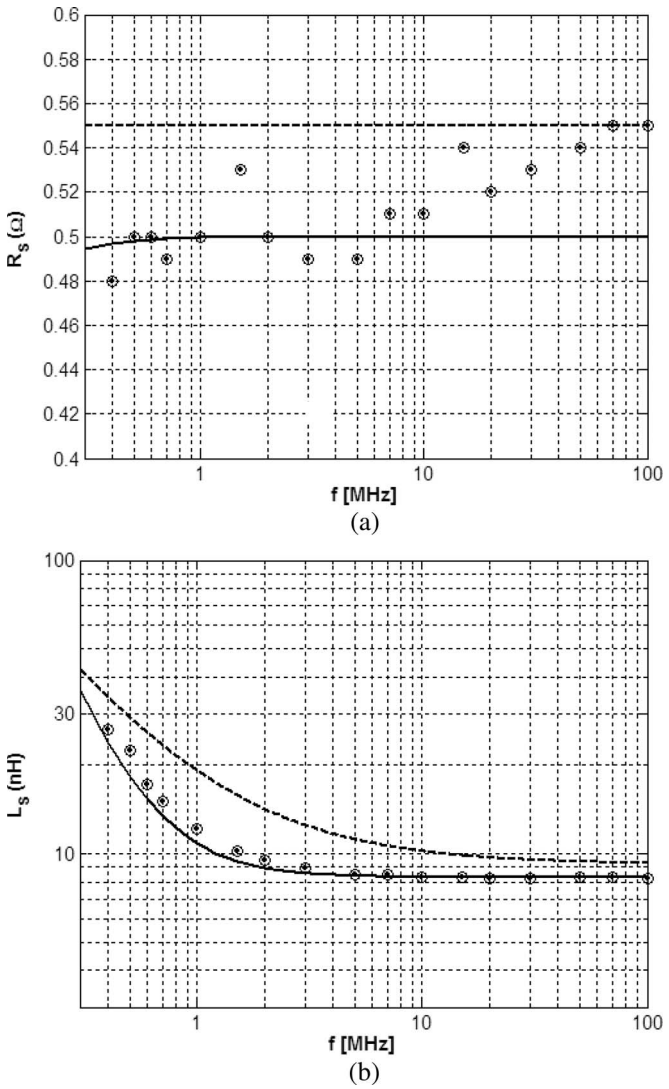

Fig. 4. Frequency behavior of the series parasitic (a) resistance and (b) inductance of the Hewlett and Packard VIM model 4193A. Dotted circles represent measured values, and continuous lines represent theoretical predictions [see (11)]. Dashed lines represent the limits given by the manufacturer. The dashed line in (b), however, includes an additive term of +4.3 nH (see text).

Substituting (8) and (4) into (7), we obtain

$$\begin{aligned} R_S+j\omega L_S &= \frac{1}{N^2}\frac{R\cdot j\omega L}{R+j\omega L}+j\omega\left(L_p-\frac{L_0}{N^2}\right) \\ &= \frac{1}{N^2}\frac{R\cdot j\omega L(R-j\omega L)}{R^2+(\omega L)^2}+j\omega\left(L_p-\frac{L_0}{N^2}\right) \\ &= \frac{R}{N^2}\frac{(\omega L)^2}{R^2+(\omega L)^2} \\ &\quad + j\omega\left[\left(L_p-\frac{L_0}{N^2}\right)+\frac{L}{N^2}\frac{R^2}{R^2+(\omega L)^2}\right] \end{aligned} \tag{9}$$

and separately equating the real and imaginary parts, we obtain

$$\begin{aligned} R_S &= \frac{R}{N^2}\frac{(\omega L)^2}{R^2+(\omega L)^2} \\ L_S &= L_S^{HF}+\frac{L}{N^2}\frac{R^2}{R^2+(\omega L)^2} \end{aligned} \tag{10}$$

where we denote as $L_S^{HF}=L_P-L_0/N^2$ the limiting value of L_S when $f\to\infty$. Substituting (5) into (10), we obtain

$$\begin{aligned} R_S &= \frac{1}{1+(f_{c1}/f)^2}\cdot\frac{R}{N^2} \\ L_S &= \frac{1+(f/f_z)^2}{1+(f/f_{c1})^2}\cdot\left(\frac{f_z}{f_{c1}}\right)^2\cdot L_S^{HF} \end{aligned} \tag{11}$$

where

$$f_z = f_{c1}\cdot\sqrt{1+1/N^2\cdot L/L_S^{HF}} \tag{12}$$

is the frequency of the zero of L_S.

The values adopted here for the parameters appearing in (11), namely, R, N, f_{c1}, and f_z, are obtained as follows: By inspection of the schematic diagrams in [11], we find $R=50\ \Omega$. From (11), we have that the high-frequency asymptotic value of R_S is R/N^2. Since the measured asymptotic value is nearly constant with increasing frequency and reasonably close to 0.5 Ω [see Fig. 4(a)], we conclude that $N=10$. The front-end circuit of the voltage-sensing channel, which is located inside the head body, is a first-order RC high-pass filter. Such filter compensates for the phase shift introduced by the current probe in the current-sensing channel. From the schematic diagrams of the VIM service manual, we find that the resistance and capacitance values of the filter are 50 Ω and 100 nF, respectively. Hence, $f_{c1}=1/(2\pi RC)=31.85$ kHz, and from (5), $L=250\ \mu$H. Finally, the value of L_S^{HF} is needed for the determination of f_z. The term L_S^{HF} depends on L_P, i.e., on the shape of the primary circuit, which is partly hidden inside the head. However, L_S^{HF} can be obtained from the asymptotic value of the measured series parasitic inductance, which gives $L_S^{HF}=8.3$ nH. The value for f_z is then readily obtained from (11) as 553.7 kHz.

Fig. 4 shows the frequency behavior of R_S and L_S as predicted from (11) (continuous line). The dotted circles represent the measurements. For clarity, the curves are plotted starting from 300 kHz, i.e., below the minimum frequency of operation of the instrument (400 kHz). Given the pole frequency f_{c1} of 31.85 kHz, R_S turns out to be constant above 400 kHz and equal to $R/N^2=0.5\ \Omega$. The measured values are practically constant and equal to about 0.5 Ω through the frequency range of operation (400 kHz to 110 MHz) with a relatively small dispersion (26 mΩ RMS over the 17 measured data, i.e., 5%), which is better than expected since we are evaluating values close to the low limit of readability. With an f_z value of 553.7 kHz, L_S starts decreasing with increasing frequency from 26.6 nH at 400 kHz, asymptotically reaching its high-frequency value L_S^{HF} of about 8.3 nH above 5 MHz. The RMS deviation between the 17 measured inductance values and the corresponding (same frequency) theoretical values is 1.4 nH. The observed behavior of the parasitic inductance confirms the validity of the model in [2]. The inductance decrease is caused by the partial cancellation of the magnetic flux in the short-circuit loop, which is produced by the current flowing in the secondary winding of the current-measuring transformer.

Further data and comments can be added on the basis of some reference values from the manufacturer. The "Supplemental

performance characteristics" (typical data, not specifications) in [11] give $R_S \leq 0.55\,\Omega$ and $L_S \leq (4.9 + 10/f)$ nH, where f is in megahertz. The R_S term appears satisfactory when compared with our theoretical and experimental data in Fig. 4(a), but the L_s term requires elaboration and discussion. It can be seen that the given limit, when plotted in Fig. 4(b), consistently falls *below* the experimental values over most of the frequency range, which is in contrast with the $\leq$ condition.[2] This discrepancy can be fixed by assuming that the manufacturer's option was to only include the contribution to L_s from the components internal to the head. Let us add a contribution from the external connection, such as the inductance of the contact pin; then, for a round conductor of 9-mm length and 1.3-mm diameter, an inductance contribution of about 4.3 nH can be estimated [12, eq. 6.21] and added to the manufacturer limit, which now gives the new limit $L_S \leq (4.9 + 4.3 + 10/f)$. This is convincingly plotted in Fig. 4(b) (dashed line). One more important discrepancy refers to the L_s variation with frequency. The limit from the manufacturer declares a $1/f$ behavior. The frequency dependence adopted in Fig. 4(b) is rather predicted as $1/f^2$ [see the second of equations (11)].

IV. Conclusion

A previously unavailable physical quantitative description of the RF current probe loading in the circuit being measured has been presented and discussed. The model for the insertion impedance of the RF current probes discussed in this paper is confirmed to be a valid tool for describing this important parameter over the frequency range of interest for the applications. Interesting applications can be, among others, 1) basic design hints, 2) accuracy evaluations and correction of errors produced by the series parasitic impedance in the analysis of measurements, or 3) incorporation of the model in automatic correction routines using experimentally or theoretically derived parameter values.

Further complexities exist, mainly in connection with the magnetic material behavior (eddy currents, hysteresis, relaxation, not to mention nonlinearity). The method developed here can help identify these unwanted aspects through correlation with the experimentally observed behavior and possibly circumventing the otherwise very heavy design task by careful choice of appropriate material and circuit parameter values.

References

[1] C. F. M. Carobbi and L. M. Millanta, "The loading effect of the radio-frequency current probes," in *Proc. 23rd Instrum. Meas. Technol. Conf.*, Sorrento, Italy, Apr. 24–27, 2006, pp. 2050–2053.

[2] L. M. Millanta, "Fundamentals of the EMC current probes," in *Proc. 12th Int. Zurich Symp. Tech. Exhib.*, Feb. 18–20, 1997, pp. 585–590.

[3] *Instruction Manual—P6022 Current Probe, 070-0948-03*, Tektronix, Beaverton, OR, 1993.

[4] *Electromagnetic Compatibility (EMC)—Part 4: Testing and Measurement Techniques, Section 6: Immunity to Conducted Disturbances, Induced by Radio-Frequency Fields*, European Standard, EN 61000-4-6:1996-07.

[5] D. C. Smith, "Current probes, more useful than you think," in *Proc. IEEE Int. Symp. EMC*, Denver, CO, Aug. 24–28, 1998, pp. 284–289.

[6] A. R. Ruddle, S. C. Pomeroy, and D. D. Ward, "Calibration of current transducers at high frequencies," *IEEE Trans. Electromagn. Compat.*, vol. 43, no. 1, pp. 100–104, Feb. 2001.

[7] G. Cerri, R. De Leo, V. M. Primiani, S. Pennesi, and P. Russo, "Wide-band characterization of current probes," *IEEE Trans. Electromagn. Compat.*, vol. 45, no. 4, pp. 616–625, Nov. 2003.

[8] Comité International Spécial des Perturbations Radioélectriques (CISPR), *Specification for Radio Disturbance and Immunity Measuring Apparatus and Methods–Part 1: Radio Disturbance and Immunity Measuring Apparatus*, CISPR 16-1, Oct. 1999.

[9] F. E. Terman, *Electronic and Radio Engineering*, 4th ed. New York: McGraw-Hill, 1995.

[10] *Instructions—A6312, 100 MHz AC/DC Current Probe, 070-9603-02*, Tektronix, Beaverton, OR.

[11] "Model 4193A vector impedance meter," *Operation and Service Manual*, Manual Part No. 04193-90000, Aug. 1983.

[12] C. R. Paul, *Introduction to Electromagnetic Compatibility*. New York: Wiley, 1992.

Carlo F. M. Carobbi (M'02) was born in Pistoia, Italy. He received the M.S. degree (*cum laude*) in electronic engineering, with a thesis on electromagnetic compatibility (EMC) problems in the power distribution network, and the Ph.D. degree in telematics, working on the physical characterization of the power distribution network as a communication medium, from the University of Florence, Florence, Italy, in 1994 and 2000, respectively.

Since 2001, he has been with the Department of Electronics and Telecommunications, University of Florence, where he was a Researcher and currently teaches courses in electrical and EMC measurements. His research activity is devoted to several aspects of EMC including EMC measurements and uncertainty evaluation and EMC-compliant design.

Luigi M. Millanta was born in Leghorn, Italy. He received the M.S. degree in electrical engineering from the University of Pisa, Pisa, Italy, in 1962.

He qualified for university teaching in microwaves in Rome, Italy, in 1969. He was with the Italian National Research Council at the Electromagnetic Waves Research Institute, Florence, Italy, from 1963 to 1984. He then joined the Department of Electronics and Telecommunications, School of Engineering, University of Florence, Florence, to teach the newly established course of electromagnetic compatibility. He also taught courses of electronic measurements from 2000 to 2007. His previous teaching activity included a course in microwave electronics for the degree in physics with the University of Florence, and a course of applied electronics with the University of Siena, Siena, Italy. He recently retired while maintaining free scientific cooperation activities with the department. His research activities include microwave solid-state components (mainly magnetostatic-wave devices), field measurements, radiation hazards, EM and perfusion hyperthermia in oncology, and several aspects of electromagnetic compatibility.

[2]This limit is not plotted in Fig. 4(b) to avoid excessive crowding. It is seen to correspond to the dashed plot minus a correction term of 4.3 nH, see explanation below.